Available online at www.sciencedirect.com
ScienceDirect
Trans. Nonferrous Met. Soc. China 31(2021) 1916−1929
Transactions of Nonferrous Metals Society of China
www.tnmsc.cn

Creep ageing behaviour assisted by electropulsing under different stresses for Al−Cu−Li alloy

Chang ZHOU[1], Li-hua ZHAN[1,2,3], He LI[3], Xing ZHAO[1,2,3], Fei CHEN[3], Ming-hui HUANG[1,2,3]

1. School of Mechanical and Electrical Engineering, Central South University, Changsha 410083, China;
2. State Key Laboratory of High-Performance Complex Manufacturing, Central South University, Changsha 410083, China;
3. Light Alloys Research Institute, Central South University, Changsha 410083, China

Received 5 June 2020; accepted 18 June 2021

Abstract: The influence of electropulsing on the creep behaviour, strength, and microstructure of an Al−Cu−Li alloy during creep ageing was investigated. Electropulsing assisted creep ageing (ECA) and conventional creep ageing (CCA) were carried out under various stress levels and time conditions. Applying electropulsing results in a noteworthy change of creep behaviour, including a variation in creep curves, an increased creep rate in early stage, and an improved creep strain. The ECA specimen experiences a shorter time to the peak strength, and an increase in elongation by ~17.4% without loss of the peak-aged strength compared with CCA specimen. The ultrafine nano-size subgrains are observed to form under electropulsing, which can result in an increased creep strain by increasing grain-boundary sliding. The enhancement of both dislocation interactions and solute diffusion under electropulsing is considered as a primary cause of disappearance of a platform stage during early creep ageing. Some of T_1 precipitates around the grain boundary are observed in the peak ECA sample, resulting in an occurrence of transgranular fracture, which is further responsible for an increased elongation of the ECA specimen.

Key words: Al−Cu−Li alloy; creep ageing; electropulsing; precipitation; microstructure

1 Introduction

The third generation aluminum−lithium (Al−Li) alloys, presenting a promising combination of properties such as low density, high strength and toughness, excellent corrosion resistance, and high specific strength, have been of great interest to the aerospace applications [1−3]. For instance, the AA2219 alloy, generally used for the cryogenic fuel tank on the space shuttle, has been gradually replaced with an AA2195 alloy, for the reason that it offers a lower density, higher modulus and strength than the AA2219 alloy [4]. In Al−Li alloy system, the ternary Al−Cu−Li alloys are more widely used in the commercial applications, and show a complex precipitation sequence, exhibiting aspects of both binary Al−Cu and Al−Li systems. The precipitation of the T_1 phase (Al_2CuLi), forming as thin plates lying on the {111} matrix planes, results in high yield strength of these Al−Cu−Li alloys [5−7]. Applying pre-strains to a material before ageing has been extensively studied and is known to produce a uniform distribution of dislocations throughout the matrix, which serve as heterogeneous nucleation sites for T_1 precipitates [8−10]. This would give rise to the nucleation of a fine homogeneous distribution of the T_1 plates within the matrix during ageing, further leading to exceptional mechanical properties [11,12].

Creep age forming (CAF) is an effective technique to form the large light weight and high

Corresponding author: Li-hua ZHAN, Tel: +86-13974874472, E-mail: yjs-cast@csu.edu.cn
DOI: 10.1016/S1003-6326(21)65626-1

performance panel products, by applying an external stress on the material at ageing temperature for a definite time, to simultaneously obtain promising mechanical properties by age hardening and plastically forming the component by creep deformation [13−16]. Much previous work has been carried out to investigate the effect of technological parameters (external stress, ageing temperature, and time, etc), on creep behaviour−microstructure−strength relationships for many age-hardening alloys, especially for Al−Cu−Li alloys. ZHANG et al [17] found that creep ageing can promote the nucleation of the T_1 plates, resulting in a fine and dense distribution of precipitates within the matrix for an AA2050 Al−Cu−Li alloy. LYU et al [18] reported that external stress can accelerate the coarsening of GP zones and η' precipitates, and promote the formation of large rod-shaped η precipitates due to the high energy sites provided by dislocation from plastic loading. The dislocation creep mechanism still plays a dominant role in the existing theory, thinking that the applied stress can introduce dislocation into the matrix during creep ageing. However, the conventional CAF would experience increasing difficulties in the achievement of forming for some of characteristic materials such as Al−Li alloys, owing to merely a little creep strain under CAF condition, which hinders the material forming. In the present research, an effective and promising method is proposed, namely creep age forming assisted by electropulsing, to control the microstructure to attain a sound material forming/property synergy.

Many researches have shown that electropulsing can signally influence the deformation behaviour, property and microstructure of metal materials. ROH et al [19] discovered that the formability of 5052-H32 Al alloy was significantly improved by electropulsing near room temperature. XIANG and ZHANG [20] reported that a high density electropulsing (103 A/mm^2 for 150 μs) can enhance the dislocation motion, so the dislocation density decreased, and that the dislocation structure was rearranged parallel to the direction of motion of the drift electrons. WANG et al [21] found that the strength increased significantly almost without loss of ductility after electropulsing was applied to an Al−Mg−Si alloy between solution and ageing process. XU et al [22] showed that electropulsing can remarkably refine the microstructure of hot-rolled 2024 aluminum through rapid recrystallization, and promote the nucleation of recrystallization. While much previous work has been carried out on electro- pulsing treatment, there has been less published on creep ageing behaviour assisted by electropulsing under different stresses.

This study aims to examine the effect of electropulsing, with optimized current parameters explored previously, on creep behaviour, strength, and microstructure relationships for an AA2195 alloy. For this purpose, creep age testing and tensile tests were used to determine the effect of electropulsing on an AA2195 alloy's creep ageing behaviour and strength after creep aged at room temperature. Scanning electron microscopy (SEM) was employed to observe the fracture morphology of the peaked specimens, in order to ascertain the cause of an improved ductility of the ECA sample. Transmission electron microscopy (TEM) was utilized to observe the refined subgrains and dislocations, and to quantify the number density and dimension of the T_1 strengthening phase. All data were employed to discuss the mechanism on pulsed current affecting creep ageing behaviour of the AA2195 alloy.

2 Experimental

2.1 Materials and solution treatment

The AA2195 alloy with chemical composition of 4.34Cu−0.95Li−0.33Mg−0.28Ag−0.15Zr (wt.%) and balance Al, as a typical Gen3 Al−Cu−Li alloy, was employed in this study. This alloy with the thickness of 8.7 mm, was supplied in a T8 temper. The dog bone-shaped creep samples with 50 mm in gage length, 15 mm in gage width and 2 mm in gage thickness, were spark machined along the roll direction from the as-received plate. All specimens were first given a solution treatment at 510 °C for 40 min and water quenched before creep ageing. Right after quenching, the samples were pre-stretched to a plastic strain of 3%. These pre-stretched specimens were then naturally aged for a week (designated here as T351 temper).

2.2 Electropulsing assisted creep ageing apparatus and procedures

The ECA apparatus was self-designed as presented in Fig. 1. The ECA test was conducted with a maximum current density (J_{max}) of

20.4 A/mm^2, a frequency (f) of 300 Hz and a duty ratio (D) of 30%, at the following steps: (1) heat the sample rapidly to the required ageing temperature (155 °C) by applying continuous pulsed current, and then load the specimen to the designated stress level during the first 1 h of the creep ageing process; (2) sequentially heat using a furnace; (3) remove the creep-aged specimen from the furnace after ECA test, and then air cooled to room temperature. The CCA test was also carried out in a similar way as a comparison. The real-time temperature of the specimen was measured by a K-type thermocouple, tightly attaching to the specimen.

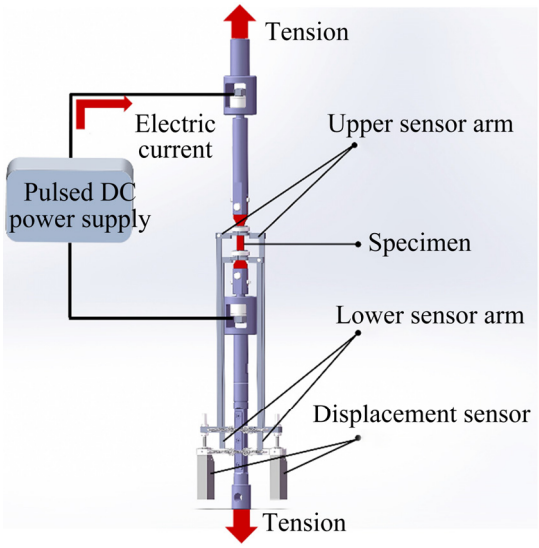

Fig. 1 Schematic diagram of electropulsing assisted creep ageing apparatus

2.3 Tensile test and microstructural characterization

Following the creep ageing, the creep aged specimens were tested to failure to examine the effect of electropulsing on the mechanical performance of material. Tensile test was carried out using an MTS Alliance RT/100 tensile apparatus at a strain rate of 2mm/min, with the strain being monitored by a 50 mm clip gauge extensometer. SEM observation was performed on a Sirion 200 scanning electron microscopy. Samples for TEM were prepared by twin-jet electropolishing using a solution of 80% methanol and 20% nitric acid at −20° under 15 V. TEM imaging was performed using a Tecnai G2 T20 microscope operating under 200 kV. Aberration-corrected scanning TEM (STEM) observation, equipped with dual CEOS aberration correctors, was carried out using a FEI Titan 80-200 FEG-TEM.

3 Results

3.1 Effect of electropulsing on creep behaviour

Figure 2 shows the creep ageing curves of the pulsed/non-pulsed specimens, under the applied stress levels of 120, 160, and 210 MPa for 20 h on the AA2195 alloy. Corresponding creep strain rate curves are also plotted for different initial stresses under the electropulsing/non-electropulsing, as presented in Fig. 3. The specimen without the assistance by electropulsing demonstrates a special creep behaviour, distinct from the conventional two-stage creep behaviour, both two particular stages with a creep strain rate of zero and respectively an increasing creep strain rate, are observed during the whole creep ageing tests. These creep ageing curves of the non-pulsed specimen under different initial stresses can be divided into four stages, based on the creep strain rate evolution, i.e., decreasing, being zero, increasing, and relatively stable creep strain rates in Fig. 3. This special four-stage creep ageing behaviour can be described as the multi-stage creep feature, as presented in Fig. 2(d). Note that the II-stage of creep ageing behaviour holds for the reducing time as a function of the increasing applied stress for the non-pulsed creep ageing tests. Surprisingly, applying electropulsing at the early stage of 1 h results in an obvious variation of creep ageing curve, compared to that of the non-pulsed specimen. These creep aged specimens subjected to electropulsing exhibit the conventional two-stage creep behaviour (see Fig. 2), which comprises a primary creep stage where creep strain rate decreases quickly and a steady-state secondary creep stage with a relatively stable creep strain rate. Namely, both II- and III-stage in the non-pulsed creep ageing curve were observed to disappear owing to the influence of electropulsing effect, which would benefit to an increase in creep deformation efficiency for the ECA specimens. On the other hand, an increase in creep strains induced by electropulsing was clearly observed under all creep ageing stress levels (120, 160, and 210 MPa), especially happening at the early creep ageing stage of ~2.5 h.

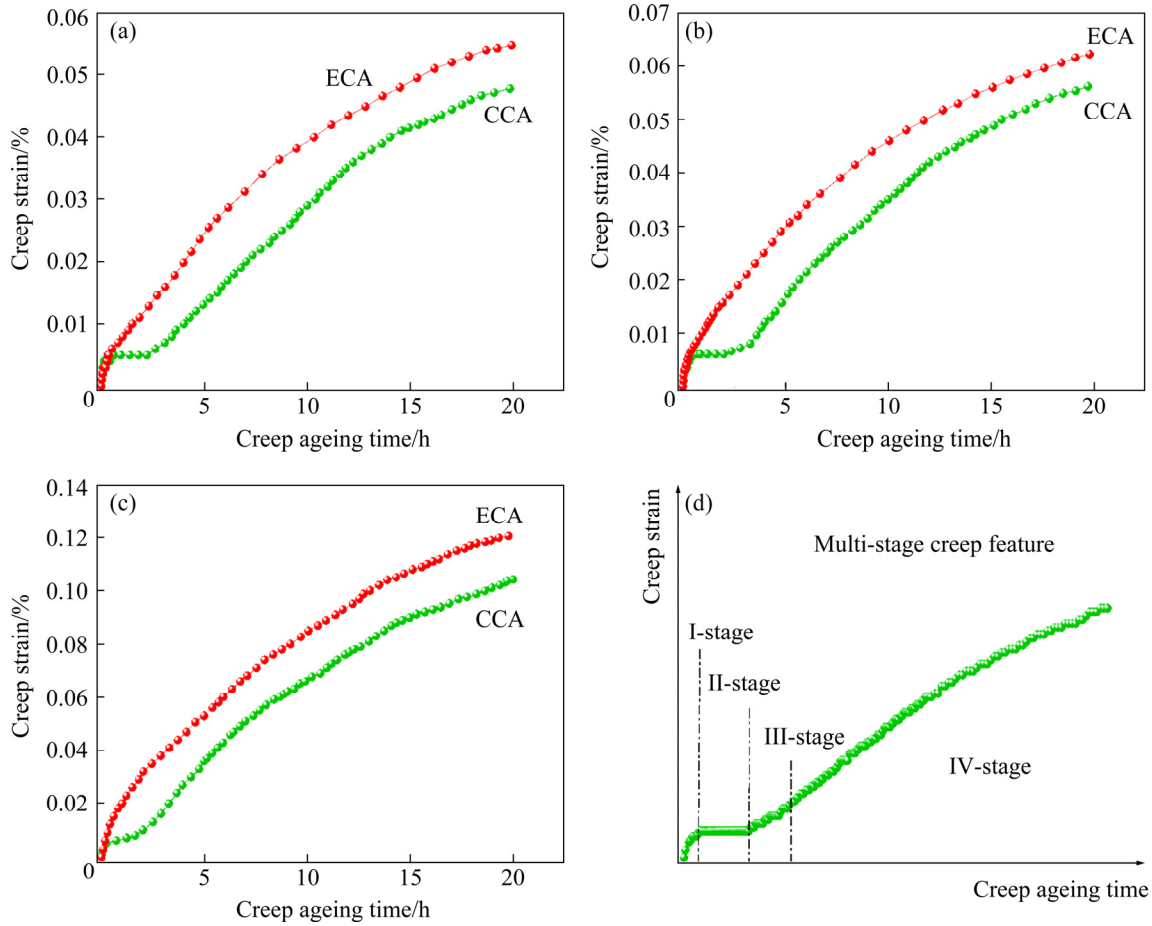

Fig. 2 Creep ageing curves of ECA/CCA specimens at ageing temperature of 155 °C for 20 h with initial stress levels of 120 MPa (a), 160 MPa (b), and 210 MPa (c), and schematic of multi-stage creep feature for AA2195 alloy with T351 initial temper (d)

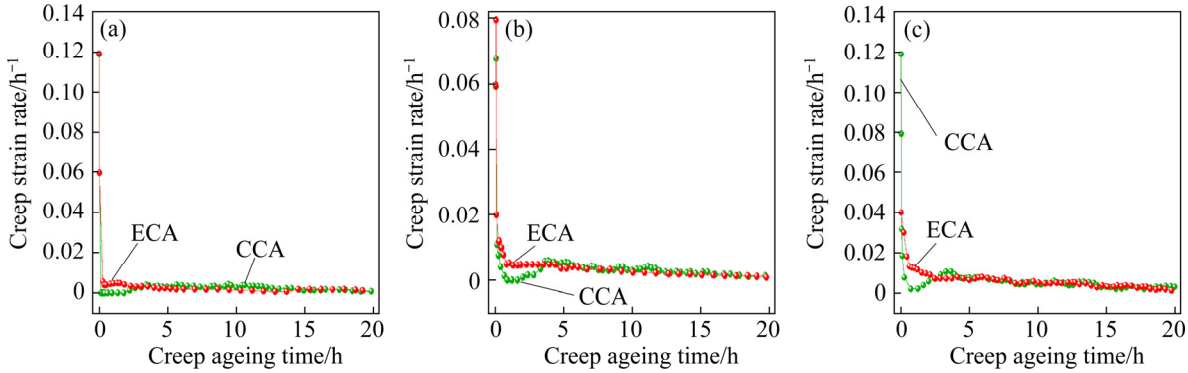

Fig. 3 Creep strain rate curves of ECA/CCA specimens at 155 °C for 20 h under different initial stresses: (a) 120 MPa; (b) 160 MPa; (c) 210 MPa

3.2 Effect of electropulsing on mechanical properties

Figure 4 shows the comparison on the evolution of average mechanical properties (from 3 tests), including yield stress, tensile strength, and elongation (plastic strain to failure), obtained from tensile testing the pulsed/non-pulsed creep aged specimens. At the initial heating ramp, a similar level of softening happens for both ECA and CCA conditions, attributing to the reversion of the solute clusters formed by natural ageing [23]. Although similar evolution trends of strength and ductility along creep ageing time were observed from the whole curves for the pulsed/non-pulsed creep aged

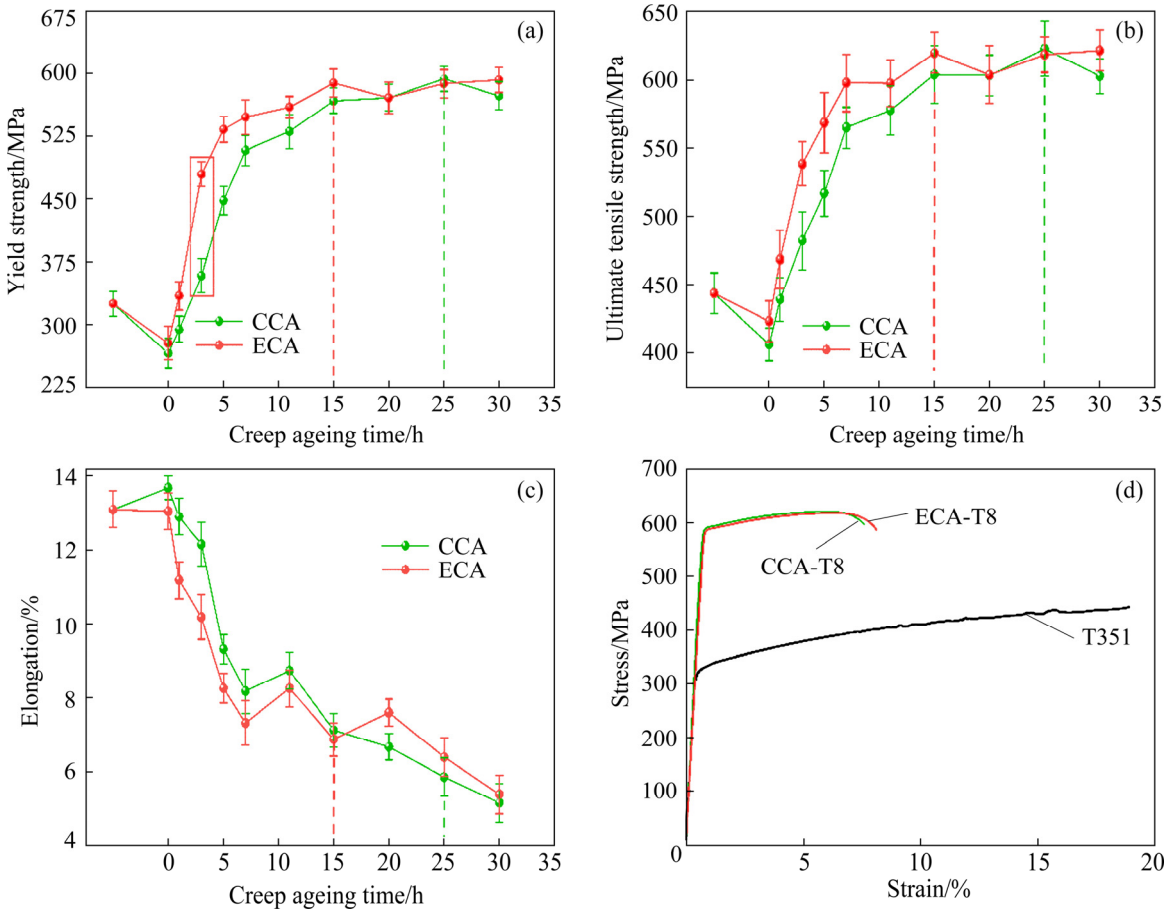

Fig. 4 Evolution of yield stress (a), ultimate tensile strength (b) and elongation (plastic strain to failure) (c) against creep ageing time for pusled/non-pulsed specimens after 210 MPa at 155 °C tension creep ageing tests, and stress−strain curves of pulsed/non-pulsed specimens in T8 condition (d)

specimens, the strength of specimens subjected to electropulsing obviously was higher than that of the non-pulsed specimen and the corresponding elongation of the pulsed specimen was lower at the same creep ageing time. With increasing creep ageing time to the peaked status, the peak strengths in both ECA and CCA conditions were almost same, but an increase of ~17.4% in peak elongation of the ECA sample was clearly observed in Fig. 4(c). Moreover, it can also be observed that the electropulsing aged specimen experiences a shorter time by around 15 h to obtain the peak strength, compared to that of CCA specimens. These results indicate an acceleration in evolution of strength and an improvement in ductility of the peaked specimen by electropulsing.

3.3 Microstructural evolution by electropulsing

HAADF-STEM imaging was employed to observe the microstructure evolution of the pulsed/non-pulsed samples with increasing creep ageing time, focusing on the behaviour of the T_1 strengthening precipitates. Examples of HAADF-STEM images of the microstructures seen in the early creep aged samples assisted by electropulsing/non-electropulsing under 210 MPa within 3 h are shown in Fig. 5, taken along a $\langle 110 \rangle_{Al}$ zone axis. Dislocations within the T351 initial temper are reasonably abundant and uniformly distributed in the form of forests [12], as the case in the alloy studied here. After 1 h creep ageing under 210 MPa, the high dislocation densities in dense forests were still observed to present throughout the aluminum matrix, and that no apparent precipitates were observed. By contrast, these samples subjected to electropulsing after creep ageing for 1 h, show the presence of a certain number density, but even smaller dimension of T_1 precipitates within the Al matrix. These high density dislocations existing within the matrix are extremely difficult to observe after the appearance of precipitates, since dislocations are masked by precipitate coherency

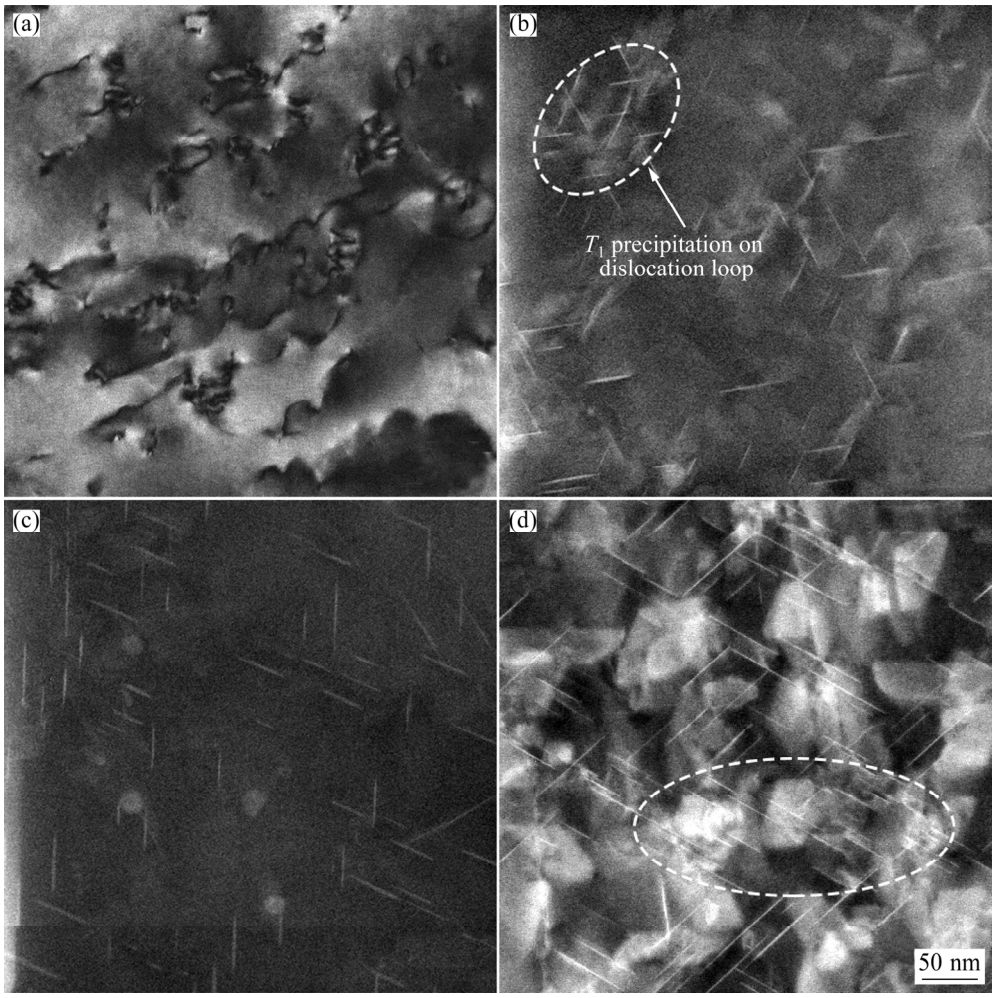

Fig. 5 HAADF-STEM images of pulsed/non-pulsed samples (close to $\langle 110 \rangle_{Al}$ zone axis), showing microstructural evolution at early stage of creep ageing (within 3 h) under 210 MPa at 155 °C, including CCA for 1 h (bright-field TEM) (a), ECA for 1 h (b), CCA for 3 h (c), and ECA for 3 h (d)

contrast, as shown in Fig. 5(b). As creep ageing goes on, a certain number density and smaller dimension of T_1 precipitates also appear in the CCA sample for 3 h. Note that from Figs. 5(b, c) the distribution of T_1 precipitates shows a distinct difference, where segregation of T_1 precipitates on some sites (considered as the tangled dislocation structures or dislocation loops here) in the form of clusters within the samples is subjected to electropulsing. Figure 5(d) shows the noteworthy growth, both in number density and dimension (at length and thickness directions) of T_1 precipitates in the ECA sample for 3 h. In addition, some of T_1 plates were also found to preferentially nucleate on some areas, and further grow to precipitate clusters as indicated by circle in Fig. 5(d). With increasing creep ageing time to the peaked status, the CCA and ECA samples present the absence of the discrepancy in T_1 precipitates, showing the presence of numerous T_1 platelets of high aspect ratio and the exceptionally uniform distribution in the material, as shown in Fig. 6.

To further acquire information on T_1 precipitation evolution induced by electropulsing from the HAADF-STEM images, the size distribution of the T_1 plates (from at least 100 precipitates in several sample areas) was manually measured by the Nano Measurer image processing software (Fig. 7). Moreover, T_1 precipitate number per unit volume (number density) was statistically analyzed for the samples aged under CCA and ECA conditions, and the results are presented in Fig. 8. These results in Figs.7 and 8 demonstrate that after creep ageing assisted by electropulsing for only 1 h the T_1 average precipitate diameter grows to be 34.5 nm and number density reaches 2.42×10^3 μm^{-3},

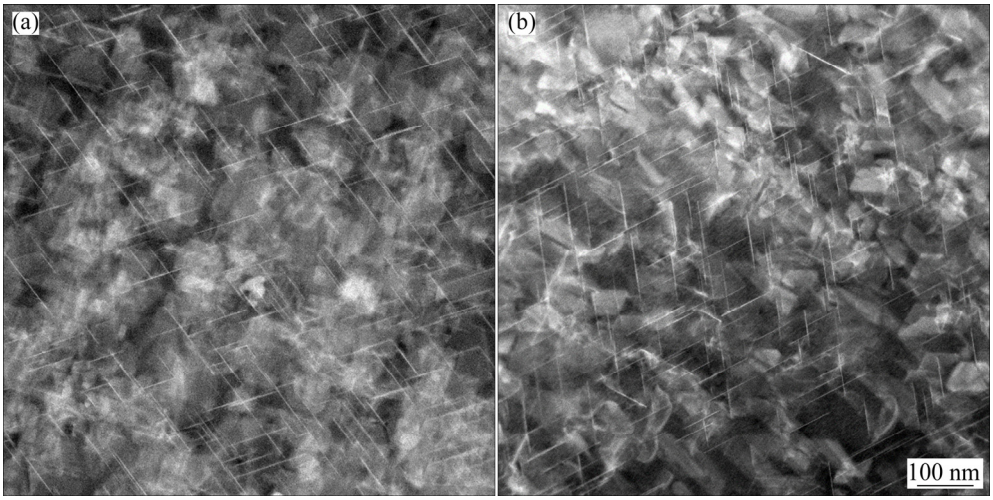

Fig. 6 HAADF-STEM images along $\langle 110 \rangle_{Al}$ zone axis, showing microstructures in peaked state of AA2195 alloy after CCA for 25 h (a) and after ECA for 15 h (b)

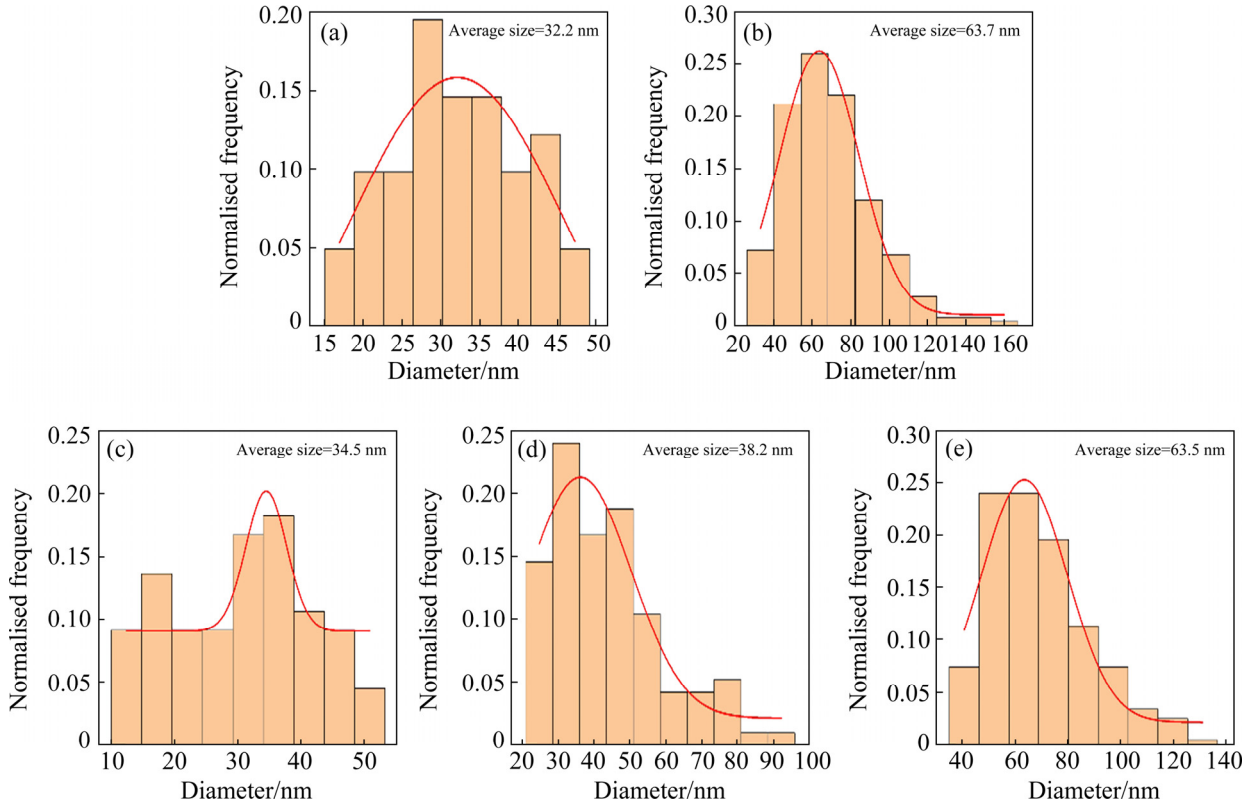

Fig. 7 Evolution of average plate diameter and size distribution of T_1 phases under different conditions after 210 MPa creep ageing tests at 155 °C: (a) CCA for 3 h; (b) CCA for 25 h (peak-aged state); (c) ECA for 1 h; (d) ECA for 3 h; (e) ECA for 15 h (peak-aged state)

which is almost equivalent to those of CCA samples aged for 3 h. And then increasing creep ageing time to 3 h, the average T_1 plate diameter measured from ECA samples further grows to be 38.2 nm, which is larger than that of CCA samples at the same ageing time. Moreover, the T_1 number density of ECA sample for 3 h, 4.87×10^3 μm^{-3}, is nearly twice as much as 2.77×10^3 μm^{-3} of CCA sample at the same time. However, the consistency in the average diameter and number density appears to happen after further creep ageing to the peaked state under CCA/ECA conditions. The above results confirm that an acceleration in the T_1 precipitation happens under the electropulsing conditions.

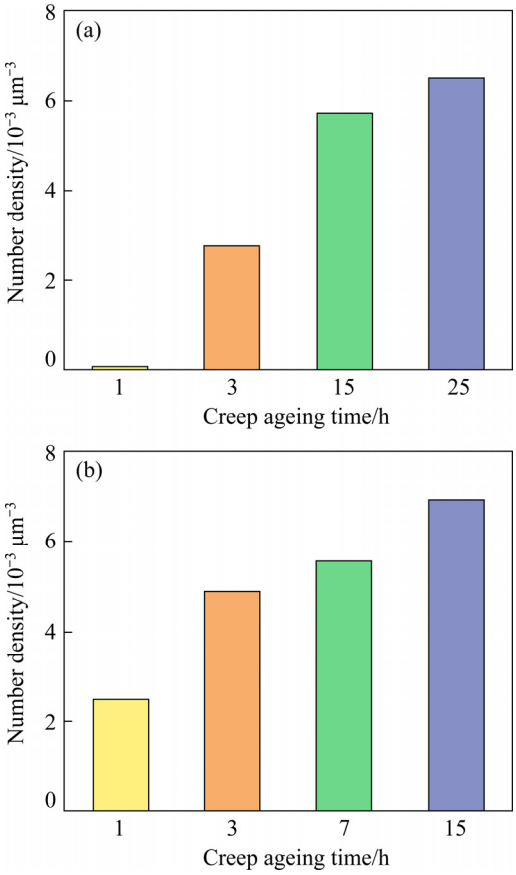

Fig. 8 Evolution of number density of T_1 precipitates within samples aged under different conditions: (a) CCA; (b) ECA

Mechanical properties of the age hardening alloy, mainly including yield strength, ultimate tensile strength and elongation, can be significantly affected by precipitates from the matrix. For the sake of simplicity, the main strengthening components can be summed by the following relationship [12]:

$$\sigma_y=M(\tau_B+\Delta\tau_\rho+\Delta\tau_P) \quad (1)$$

where σ_y is the yield strength of the material, τ_B is the constant base shear strength, $\Delta\tau_\rho$ and $\Delta\tau_P$ are the increase of strength attributing to strain hardening and precipitation, respectively, and M is the Taylor factor.

The quantitative analysis of the effect of second phase particles, mainly precipitates within the grains, on mechanical properties of metallic materials can be expressed from Refs. [12,24]:

$$\Delta\tau_P=\frac{1.211D^2\gamma_{eff}^{3/2}}{\sqrt{t^3}}\cdot\sqrt{\frac{\pi bN}{4\Gamma}} \quad (2)$$

where D is the average diameter; t is the thickness; γ_{eff} is an effective interfacial energy term that considers both the interfacial and stacking fault energy contribution associated with shearing a precipitate; b is the magnitude of Burgers vector, N is the number density of the T_1 precipitates, and Γ is the dislocation line tension. Note that Eq. (2) is only applicable for the T_1 precipitates strengthened alloys in the under-aged and peak-aged conditions.

From Eqs. (1) and (2), the contribution of precipitation on the yield stress of materials thus mainly depends on the average diameter (D) and the number density (N) of T_1 phases, i.e., increasing with these two components. At the creep ageing time of 3 h, both the average diameter and number density of ECA sample are much larger than those of the CCA sample, which accounts for yield strength of ECA sample exceeding over ~120 MPa comparing with that of CCA sample (highlighted by red rectangle in Fig. 4(a)). Besides, nearly the same average diameter and number density of the two peak-aged samples also correspond to the no difference in strength in Fig. 4. According to Eqs. (1) and (2), the evolution of the average plate diameter and number density of T_1 precipitates during CCA/ECA is in line with the variation of strength in Fig. 4.

3.4 Effect of electropulsing on fracture behaviour

To determine the cause of an increase in elongation induced by electropulsing without loss of strength for the peak-aged specimen, fractographs were obtained for all creep aged specimens after tensile deformation to fracture. The entire fracture surfaces of sample at T351 initial temper were covered with a large amount of dimple, closely related to the sound ductility, after the uniaxial tensile test (Fig. 9(a)), suggesting a large elongation at this temper. After creep ageing from T351 temper to the peak state, the brittle intergranular separation with river line patterns was clearly observed after fracture as presented in Fig. 9(b). Surprisingly, transgranular fracture morphology was found to form in the ECA specimens for the peak state, which may be responsible for an increase in peak elongation induced by electropulsing. The feature of transgranular fracture observed in ECA specimens may be caused by segregation of precipitates at the grain boundaries.

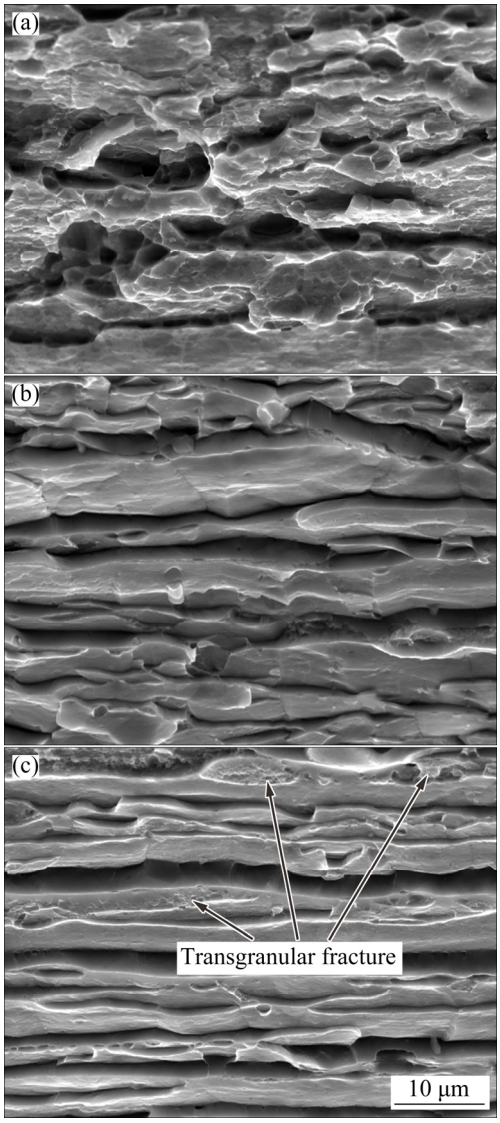

Fig. 9 Fracture surfaces after uniaxial tensile test of T351 initial temper sample (a), peak CCA sample (b), and peak ECA sample (c)

4 Discussion

Viewed from the overall, these results above show that applying electropulsing at the initial creep ageing stage of 1 h, has a significant impact on the creep ageing behaviour, mechanical properties, and microstructures of the AA2195 alloy. For examples, electropulsing induced the disappearance of II- and III-stage seen in the conventional creep ageing curves and an increase in creep strains, which would significantly improve the efficiency of creep deformation during creep age forming. Electropulsing also could induce a strong increase in formability during uniaxial tension of 5052-H32 alloy, and the recovery of dislocation occurs at a given current density [25]. The tensile test results indicate both an acceleration in creep ageing to the peak-aged state and an improvement in elongation without loss of strength by electropulsing. From HAADF STEM images, an acceleration in T_1 precipitation kinetics by electropulsing was observed for the same creep ageing time, including the larger dimension and number density than those of the CCA samples. However, XIAO et al [26] found that the combination of EPT and pre-deformation could dramatically increase the strength of 5A90 Al−Li alloy with a slight decrease in elongation with increasing the size and volume fraction of δ' phase. Although the accelerated recrystallization of cold-worked metals would occur during annealing with high or low density electropulsing [27], it was for the first time found that electropulsing can induce to form nano-sized subgrains within ageing temperatures in this study. As will be discussed further below, the mechanism in the effect of electropulsing on creep ageing behaviour of the AA2195 alloy.

Electron wind force is considered as the dominant component of the athermal effect of electropulsing, resulting from the momentum transfer between the drift electrons and metal ion cores. Many researches have shown that electron wind force can facilitate dislocation motion and solute atom diffusion. Currently, there are two more acceptable models of the electron wind force exerted by drift electrons on dislocations [28,29]. Based on consideration of the specific dislocation resistivity, the electron wind force per unit length of dislocation (F_{ew}) is given by

$$F_{ew}=\rho_D e n_e J/N_D \tag{3}$$

where ρ_D/N_D is the specific dislocation resistivity, e is the electron charge, n_e is the electron density, and J is the current density.

While the other based on the quantum mechanics considerations of the interaction between drift electrons and dislocations, gives

$$F_{ew}=\alpha b p_F(J/e-n_e v_D) \tag{4}$$

where α is a constant ranging between 0.1 and 1.0 depending on the details of the Fermi surface and the calculations, p_F is the Fermi momentum, and v_D is the dislocation velocity. From Eqs. (3) and (4), the utility of electron wind force largely depends on

the amplitude of current density, and increases with the rise of amplitude. ZHU et al [30] found that the electron wind force pushed the dislocation lines, which moved along the electron drift direction toward the subgrain boundaries. XIANG and ZHANG [20] also discovered that the electron wind force exerted on the dislocations can rearrange dislocation structure, which is parallel to the direction of drift electrons. Considering that Joule heating is concomitant with electron wind force, Joule heat is used for heating the specimen to the ageing temperature of 155 °C, which aims to play an electron wind force effect in this study.

From the microstructural results of the CCA and ECA samples in Section 3.3, this special multi-stage creep feature could be thought to be explained by both dislocation and diffusion mechanisms, including dislocations motion, solid solutes evolution and precipitates [31,32]. Schematic illustration in Fig. 10(a) shows the microstructural evolution of the non-pulsed specimens during 210 MPa creep ageing test at 155 °C. After the first 0.5 h of creep ageing tests, introducing dislocations by creep deformation would be considered to reach a saturation status at the applied stress level of 210 MPa, leading to the primary creep stage (I-stage) with a promptly decreasing creep strain rate. Simultaneously, segregation of solute atoms to the dislocations begins to happen during this period, preferentially in the regions where the dislocations are most curved. Compared to the end of I-stage, significantly more segregation of solute atoms towards around the dislocations could grow to solute atmospheres pinned dislocations, which is thought to be mainly responsible for the II-stage with a creep strain rate of zero. During the III-stage with an increasing creep strain rate, solute atoms would be fast depleted by the accelerated nucleation of T_1 precipitates around the dislocations, and further to form the T_1 precursors, contributing to a decrease in the creep resistance of the materials. The microstructure, at the end of III-stage, consists of dislocations with T_1 precursors attached and a low density of small T_1 platelets nucleated at early stage (II-stage). This behaviour at the III-stage can thus be contributed to the solute-depletion softening exceeding the age hardening effect of the T_1 precursors. With increasing creep ageing time to the IV-stage, further growth of T_1 precipitates from its precursors would produce strong resistance to the motion of dislocations, contributing to a decrease in creep strain rate to the relatively stable level, IV-stage determined by T_1 precipitation. As it is solutes diffused towards the dislocations at II-stage, increasing the applied stress level increases the density of dislocations, resulting in a reduction of the average diffusion field size, so II-stage experiences a short timescale.

Schematic illustration in Fig. 10(b) shows the microstructural evolutions during 210 MPa creep ageing tests assisted by electropulsing at 155 °C. Reaching a saturation level of dislocations by creep deformation, was also considered to be mainly responsible for a fast decreasing creep strain rate during the early creep ageing stage. Different kinds

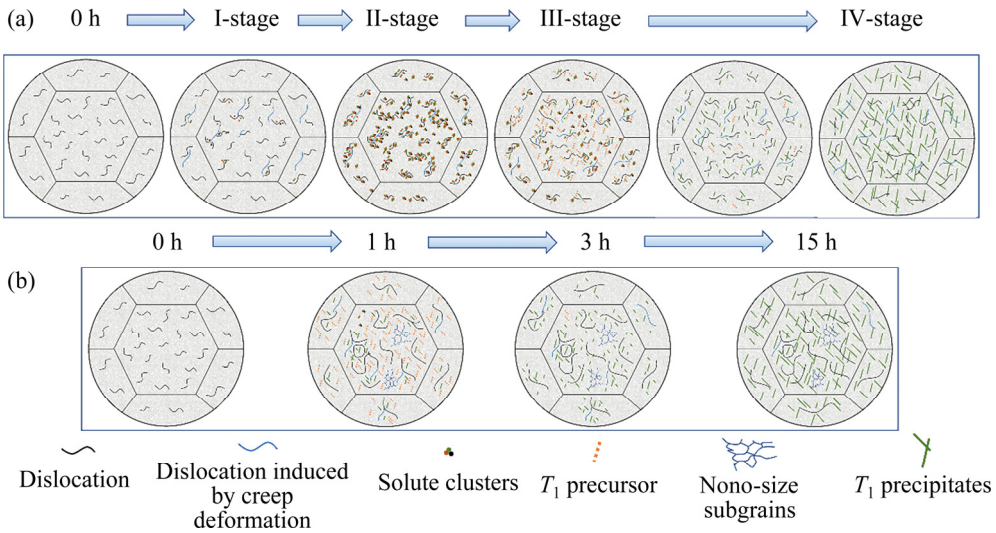

Fig. 10 Schematic illustration showing evolution of microstructures in CCA specimen (a) and ECA specimen (b) during creep ageing tests

of dislocations can react with each other to give coalescing, rearrangement in the thermal activation [33,34]. Applying electropulsing during the early stage of 1 h can lead to an enhanced interaction of dislocations, further resulting in the formation of larger dislocation structures by coalescence each other, even including some tangled dislocation structures and dislocation loops. Meanwhile, an accelerated nucleation of T_1 precipitates occurs around the high energy sites offered by the large dislocation structures, attributing to an increasing diffusion of solute atoms by electron wind force. Hence, some of T_1 plates preferentially precipitated on the high energy sites, such as dislocation loops, were observed after electropulsing aged only for 1 h. Forming a balanced relation between more difficulties for the movement of these large dislocation structures and solute-depletion softening is mostly responsible for a transient steady creep stage during the early creep ageing stage between 0.5 and ~2 h. After that creep behaviour, experiencing a slight decrease in creep strain rate until it reaching a stable level, would be dominant by the growth of T_1 precipitates, as provided stronger resistance to the movement of dislocations. Furthermore, the formation of nano-sized subgrain structures (see Fig. 11(b)) induced by electropulsing is thought to be one of causes of an increased creep strain within the initial creep stage of 3 h, since increasing grain-boundary sliding by this structure, besides attributing to an enhanced interaction of dislocations by electropulsing.

Based on comparison of number density and dimension of T_1 precipitates for both creep ageing conditions at the same creep ageing time, significantly high strength of ECA specimen than that of CCA specimen attributes to an acceleration in T_1 precipitation by electropulsing. Further, this accelerated precipitation behaviour can be attributed to the combined effect between those larger dislocation structures and the enhanced diffusion of solid solutes under electropulsing condition. Results from TEM images of grain boundary in Fig. 12 show some of T_1 precipitation at the grain boundary, resulting in an improved strength of grain boundary. This would lead to form the feature of transgranular fracture observed in the ECA specimens after tensile deformation to fracture. In other words, at the peak-aged state, almost little influence of electropulsing on intracrystalline T_1 precipitates but inducing some of T_1 precipitation at the grain boundary, which is responsible for an increased elongation by ~17.4% without loss of the peak strength than that of CCA specimen.

5 Conclusions

(1) For the ECA specimens, the disappearance of II- and III-stage in the conventional creep ageing curves and increased creep strains would significantly improve the efficiency of creep deformation during creep age forming. New insight into the multi-stage creep feature consisting of four creep stages was proposed for the AA2195 alloy.

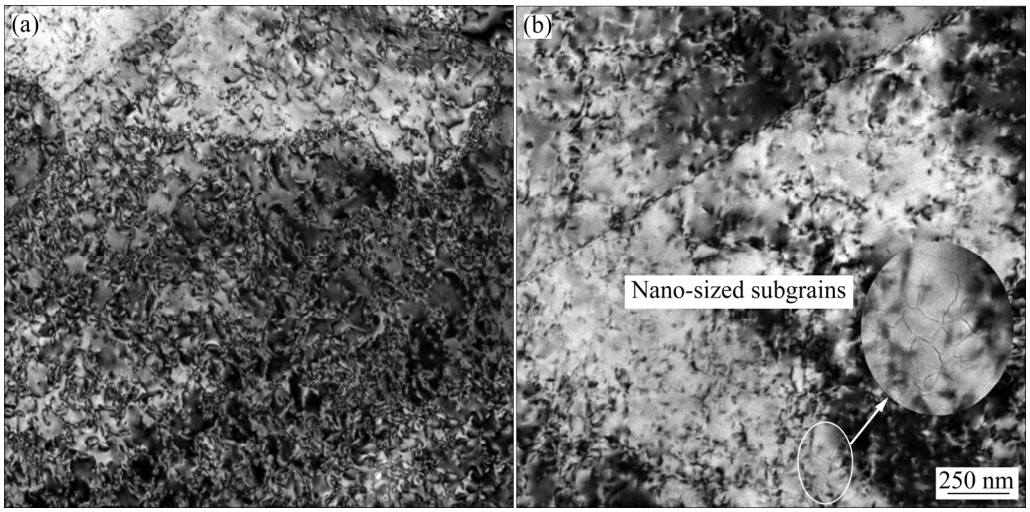

Fig. 11 Bright field TEM images showing nano-size grain structures induced by electropulsing: (a) Without applying electropulsing after 210 MPa creep ageing test for 1 h; (b) Specimen subjected to electropulsing for 1 h

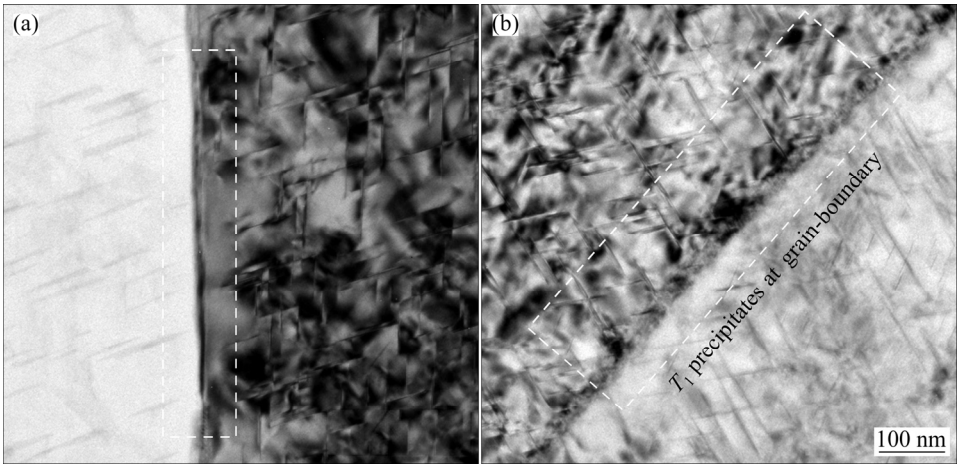

Fig. 12 TEM images at peak-aged state (close to $\langle 110 \rangle_{Al}$ zone axis) for CCA (a) and ECA (b) samples, mainly showing part segregation of T_1 precipitates at grain boundary by electropulsing

The I-, II- and III-stage are controlled by interaction of dislocations and solid solutes, and the IV-stage is controlled by the further growth of the T_1 precipitates.

(2) The tensile test results indicate both an acceleration in creep ageing to the peak-aged state and an improved elongation without loss of strength for the ECA specimens. Transgranular fracture morphology was found to form in the ECA specimens at the peak state, which may be responsible for an increase in peak elongation induced by electropulsing.

(3) This creep ageing behaviour under electropulsing can be attributed to the combined effects between those large dislocation structures and the enhanced diffusion of solid solutes. Besides, the formation of ultrafine nano-sized subgrain structures induced by electropulsing is thought to one of causes of a significant increase in creep strains within the initial creep stage of 3 h. Inducing some of T_1 precipitation at the grain boundary by electropulsing, is responsible for the occurrence of this transgranular fracture.

Acknowledgments

The authors are grateful for the financial supports by the National Key R&D Program of China (No. 2017YFB0306300), and the National Natural Science Foundation of China (Nos. 51601060, 51675538).

References

[1] RIOJA R J, LIU J. The evolution of Al−Li base products for aerospace and space [J]. Metallurgical and Materials Transactions A, 2012, 43(9): 3325−3337. https://doi.org/10.1007/s11661-012-1155-z.

[2] WARNER T. Recently-developed aluminium solutions for aerospace applications [J]. Materials Science Forum, 2006, 519−521: 1271−1278. https://doi.org/10.4028/www.scientific.net/MSF.519-521.1271.

[3] EI-ATY A A, XU Yong, GUO Xun-zhong, ZHANG Shi-hong, MA Yan, CHEN Da-yong. Strengthening mechanisms, deformation behavior, and anisotropic mechanical properties of Al−Li alloys: A review [J]. Journal of Advanced Research, 2018, 10: 49−67. https://doi.org/10.1016/j.jare.2017.12.004.

[4] DURSUN T, SOUTIS C. Recent developments in advanced aircraft aluminum alloys [J]. Materials & Design, 2014, 56: 862−871. https://doi.org/10.1016/j.matdes.2013.12.002.

[5] KANG S J, KIM T H, YANG C W, LEE J I, PARK E S, NOH T W, KIM M. Atomic structure and growth mechanism of T_1 precipitate in Al−Cu−Li−Mg−Ag alloy [J]. Scripta Materialia, 2015, 109: 68−71. https://doi.org/10.1016/j.scriptamat.2015.07.020.

[6] MA Yun-long, LI Jin-feng, ZHANG Run-zhe, TANG Jian-guo, HUANG Cheng, LI Hong-ying, ZHENG Zhi-qiao. Strength and structure variation of 2195 Al−Li alloy caused by different deformation processes of hot extrusion and cold-rolling [J]. Transactions of Nonferrous Metals Society of China, 2020, 30: 835−849. https://doi.org/10.1016/S1003-6326(20)65258-X.

[7] YANG Qing-bo, DENG Yan-jun, YANG Mou, ZHANG Zhi-qing, LI Wei-guo, LIU Qing. Effect of Al_3Zr particles on hot-compression behavior and processing map for Al−Cu−Li based alloys at elevated temperatures [J]. Transactions of Nonferrous Metals Society of China, 2020, 30: 872−882. https://doi.org/10.1016/S1003-6326(20)65261-X.

[8] PINGER S P, MUDDLE B C, POLMEAR I J. Effects of cold work on precipitation in Al−Cu−Mg−(Ag) and AI−Cu−Li−(Mg−Ag) alloys [J]. Metallurgical and Materials Transactions A, 1995, 26: 1659−1671. https://doi.org/10.1007/BF02670753.

[9] CASSADA W A, SHIFLET G J, STARKE JR E A. The effect of plastic deformation on Al_2CuLi (T_1) precipitation [J]. Metallurgical Transactions A, 1991, 22: 299−306. https://doi.org/10.1007/bf02656799.

[10] GABLE B M, ZHU A W, CSONTOS A A, STARKE JR E A. The role of plastic deformation on the competitive microstructural evolution and mechanical properties of a novel Al−Li−Cu−X alloy [J]. Journal of Light Metals, 2001, 1: 1−14. https://doi.org/10.1016/s1471-5317(00)00002-x.

[11] DORIN T, DESCHAMPS A, GEUSER F D, SIGLI C. Quantification and modelling of the microstructure/strength relationship by tailoring the morphological parameters of the T_1 phase in an Al−Cu−Li alloy [J]. Acta Materialia, 2014, 75: 134−146. https://doi.org/10.1016/j.actamat.2014.04.046.

[12] RODGERS B I, PRANGNELL P B. Quantification of the influence of increased pre-stretching on microstructure-strength relationships in the Al−Cu−Li alloy AA2195 [J]. Acta Materialia, 2016, 108: 55−67. https://doi.org/10.1016/j.actamat.2016.02.017.

[13] ZHAN Li-hua, LIN Jian-guo, DEAN T A. A review of the development of creep age forming: Experimentation, modelling and applications [J]. International Journal of Machine Tools and Manufacture, 2011, 51(1): 1−17. https://doi.org/10.1016/j.ijmachtools.2010.08.007.

[14] WANG Kai, ZHAN Li-hua, YANG You-liang, MA Zi-yao, LI Xi-cai, LIU Jian. Constitutive modeling and springback prediction of stress relaxation age forming of pre-deformed 2219 aluminum alloy [J]. Transactions of Nonferrous Metals Society of China, 2019, 29: 1152−1160. https://doi.org/10.1016/S1003-6326(19)65023-5.

[15] LIU Chun-hui, YANG Jian-shi, MA Pei-pe, MA Zi-yao, ZHAN Li-hua, CHEN Kai-liang, HUANG Min-hui, LI Jian-jun, LI Zi-ming. Large creep formability and strength-ductility synergy enabled by engineering dislocations in aluminum alloys [J]. International Journal of Plasticity, 2020, 134: 102774. https://doi.org/10.1016/j.ijplas.2020.102774.

[16] LI He, ZHAN Li-hua, HUANG Ming-hui, ZHAO Xing, ZHOU Chang. Investigation on the asymmetric creep ageing behaviour of 2195-T84 Al−Li alloy under different tensile and compressive stress levels [J]. Intermetallics, 2021, 131: 107078. https://doi.org/10.1016/j.intermet.2020.107078.

[17] ZHANG Jin, WANG Cheng, ZHANG Yong, DENG Yun-lai. Effects of creep aging upon Al−Cu−Li alloy: Strength, toughness and microstructure [J]. Journal of Alloys and Compounds, 2018, 764: 452−459. https://doi.org/10.1016/j.jallcom.2018.06.103.

[18] LYU F G, LI Yong, SHI Zhu-sheng, HUANG Xia, ZENG Yuan-song, LIN Jian-guo. Stress and temperature dependence of stress relaxation ageing behaviour of an Al−Zn−Mg alloy [J]. Materials Science and Engineering A, 2020, 773: 138859. https://doi.org/10.1016/j.msea.2019.138859.

[19] ROH J H, SEO J J, HONG S T, KIM M J, HAN H N, ROTH J T. The mechanical behavior of 5052-H32 aluminum alloys under a pulsed electric current [J]. International Journal of Plasticity, 2014, 58: 84−99. https://doi.org/10.1016/j.ijplas.2014.02.002.

[20] XIANG Si-qi, ZHANG Xin-fang. Dislocation structure evolution under electroplastic effect [J]. Materials Science and Engineering A, 2019, 761: 138026. https://doi.org/10.1016/j.msea.2019.138026.

[21] WANG Yi-tong, ZHAO Yu-guang, XU Xiao-feng, PAN Dong, JIANG Wen-qiang, YANG Xue-hui, WANG Zhe. Superior mechanical properties induced by the interaction between dislocations and precipitates in the electro-pulsing treated Al−Mg−Si alloys [J]. Materials Science and Engineering A, 2018, 735: 154−161. https://doi.org/10.1016/j.msea.2018.08.029.

[22] XU Xiao-feng, ZHAO Yu-guang, MA Bing-dong, ZHANG Jia-tao, ZHANG Ming. Rapid grain refinement of 2024 Al alloy through recrystallization induced by electropulsing [J]. Materials Science and Engineering A, 2014, 612: 223−226. https://doi.org/10.1016/j.msea.2014.06.057.

[23] DECREUS B, DESCHAMPS A, GEUSER F D, DONNADIEU P, SIGLI C, WEYLAND M. The influence of Cu/Li ratio on precipitation in Al−Cu−Li−x alloys [J]. Acta Materialia, 2013, 61(6): 2207−2218. https://doi.org/10.1016/j.actamat.2012.12.041.

[24] HUANG Ke, MARTHINSEN K, ZHAO Qing-long, LOGÉ R E. The double-edge effect of second-phase particles on the recrystallization behaviour and associated mechanical properties of metallic materials [J]. Progress in Materials Science, 2018, 92: 284−359. https://doi.org/10.1016/j.pmatsci.2017.10.004.

[25] KIM M J, LEE K, OH K H, CHOI I S, YU H H, HONG S T, HAN H N. Electric current-induced annealing during uniaxial tension of aluminum alloy [J]. Scripta Materialia, 2014, 75: 58−61. https://doi.org/10.1016/j.scriptamat.2013.11.019.

[26] XIAO Han, ZHANG Kai-feng, SHI Cheng-cheng, LU Zhen, JIANG Ju-fu. Influence of electropulsing treatment combined with pre-deformation on ageing behavior and mechanical properties of 5A90 Al−Li alloy [J]. Journal of Alloys and Compounds, 2019, 784: 1234−1247. https://doi.org/10.1016/j.jallcom.2019.01.103.

[27] HUANG Ke, CAYRON C, LOGE R E. The surprising influence of continuous alternating electric current on recrystallization behaviour of a cold-rolled Aluminium alloy [J]. Materials Characterization, 2017, 129: 121−126. https://doi.org/10.1016/j.matchar.2017.04.036.

[28] CONRAD H, SPRECHER A F, CAO W D, LU X P. Electroplasticity—The effect of electricity on the mechanical properties of metals [J]. JOM, 1990, 49: 28−33. https://doi.org/10.1007/BF03220478.

[29] CONRAD H. Thermally activated plastic flow of metals and ceramics with an electric field or current [J]. Materials Science and Engineering A, 2002, 322: 100−107. https://doi.org/10.1016/S0921-5093(01)01122-4.

[30] ZHU Y H, TO S, LEE W B, LIU X M, JIANG Y B, TANG G Y. Effects of dynamic electropulsing on microstructure and elongation of a Zn−Al alloy [J]. Materials Science and Engineering A, 2009, 501: 125−132. https://doi.org/10.1016/j.msea.2008.09.080.

[31] LI Y, SHI Z, LIN J, YANG Y L, HUANG B M, CHUNG T F, YANG J R. Experimental investigation of tension and compression creep-ageing behavior of AA2050 with different initial tempers [J]. Materials Science and

Engineering A, 2016, 657: 299−308. https://doi.org/10.1016/j.msea.2016.01.074.

[32] ZHOU Chang, ZHAN Li-hua, SHEN Ru-lin, ZHAO Xing, YU Hai-liang, HUANG Ming-hui, LI He, YANG You-liang, HU Li-bin, LIU De-bo, HU Zheng-gen. Creep behavior and mechanical properties of Al−Li−S4 alloys at different aging temperatures [J]. Journal of Central South University, 2020, 27: 1168−1175. https://doi.org/10.1007/s11771-020-4357-3.

[33] LIU Chun-hui, MALLADI S K, XU Qiang, CHEN Jiang-hua, TICHELAAR F D, ZHUGE Xiao-dong, ZANDBERGEN H W. In-situ STEM imaging of growth and phase change of individual $CuAl_X$ precipitates in Al alloy [J]. Scientific Reports, 2017, 7(1): 2184. https://doi.org/10.1038/s41598-017-02081-9.

[34] ZHANG W, SUI M L, ZHOU Y Z, LI D X. Evolution of microstructures in materials induced by electropulsing [J]. Micron, 2003, 34(3−5): 189−198. https://doi.org/10.1016/S0968-4328(03)00025-8.

Al−Cu−Li 合金在不同应力下的电脉冲辅助蠕变时效行为

周 畅[1]，湛利华[1,2,3]，李 贺[3]，赵 兴[1,2,3]，陈 非[3]，黄明辉[1,2,3]

1. 中南大学 机电工程学院，长沙 410083；
2. 中南大学 高性能复杂制造国家重点实验室，长沙 410083；
3. 中南大学 轻合金研究院，长沙 410083

摘 要：研究电脉冲对 Al−Cu−Li 合金蠕变时效行为、强度和显微组织的影响。在不同的应力和时间条件下，进行电脉冲辅助蠕变时效(ECA)和常规蠕变时效(CCA)实验。施加电脉冲可以显著改变合金的蠕变行为，包括蠕变曲线的变化、初期蠕变速率的增加和蠕变量的提高。ECA 试样达到峰值强度的时间比 CCA 试样的短，在强度几乎不变的情况下，其伸长率提高约 17.4%。在电脉冲作用下，晶粒细化导致形成超细纳米级亚晶粒，从而增加晶界滑动，提高蠕变量。电脉冲作用下位错相互作用和溶质原子扩散的增强被认为是蠕变早期平台阶段消失的主要原因。在峰时效 ECA 样品中观察到一些 T_1 相在晶界附近析出，这将导致穿晶断裂的发生，进而提高试样的伸长率。

关键词：Al−Cu−Li 合金；蠕变时效；电脉冲；析出；显微组织

(Edited by Xiang-qun LI)